

Sub-millimeter to centimeter excess emission from the Magellanic Clouds.

I. Global spectral energy distribution.

F.P. Israel¹, W.F. Wall², D. Raban¹, W.T. Reach³, C. Bot⁴, J.B.R. Oonk¹, N. Ysard⁵ and J.P. Bernard⁶

¹ Sterrewacht Leiden, Leiden University, P.O. Box 9513, 2300 RA Leiden, The Netherlands

² Instituto Nacional de Astrofísica, Óptica, y Electrónica, Apdo. Postal 51 y 216, Puebla, Pue., México;

³ Spitzer Science Center, California Institute of Technology, Pasadena, CA, USA

⁴ UMR7550, Observatoire Astronomique de Strasbourg, Université Louis Pasteur, F-67000 Strasbourg, France

⁵ Department of Physics, P.O. Box 64, FIN-00014 University of Helsinki, Finland

⁶ Université de Toulouse, UPS, CESR, F-31028 Toulouse, France

Received ????: accepted ????

ABSTRACT

Aims. Our goal is to determine and study the global emission from the Magellanic Clouds over the full radio to ultraviolet spectral range.

Methods. We have selected from the literature those flux densities that include the entire LMC and SMC respectively, and we have complemented these with maps extracted from the WMAP and COBE databases covering the missing the 23–90 GHz (13–3.2 mm) and the poorly sampled 1.25–250 THz (240–1.25 μm) spectral ranges in order to reconstruct the global SEDs of the Magellanic Clouds over eight decades in frequency or wavelength.

Results. A major result is the discovery of a pronounced excess of emission from the Magellanic Clouds at millimeter and sub-millimeter wavelengths. We also confirm global mid-infrared (12 μm) emission suppression, and determine accurate thermal radio fluxes and very low global extinctions for both LMC and SMC, the latter being the most extreme in all these respects.

Conclusions. These and other dust properties such as the far-UV extinction curve appear to be correlated with (low) metallicity. Possible explanations are briefly considered. As long as the nature of the excess emission is unknown, the total dust masses and gas-to-dust ratios of the Magellanic Clouds cannot reliably be determined

Key words. Galaxies – Magellanic Clouds – Sub-millimeter: galaxies – Radio continuum: galaxies – Magellanic Clouds: ISM – ISM: dust, extinction

1. Introduction

The global spectral energy distribution (SED) of entire galaxies provides an important tool to study global properties, such as star formation activity, ISM heating and cooling balance, extinction and dust content. Understanding the SEDs of nearby galaxies is essential to the interpretation of measurements of very distant galaxies. Especially important galaxies to study are the Large Magellanic Cloud (LMC) and the Small Magellanic Cloud (SMC), the southern hemisphere Milky Way satellites. They are so close (LMC: $D = 50$ kpc, SMC: $D = 63$ kpc) that we can study them in exhaustive detail allowing us to relate global to local properties. However, their very proximity gives them very large angular extent (LMC: 8° , SMC: 2°), so that global flux densities have been determined only in the relatively recent past, and over limited wavelength ranges. Particularly lacking is coverage over a broad spectral range from the far infrared (typically 2–3 THz or 0.10–0.14 mm) to the radio regime (typically 5–10 GHz or 3–6 cm). This includes the mm/submm wave region that may reveal unique information on properties and emission mechanisms of dust

as well the thermal free-free emission from ionised gas resulting from the star formation processes.

Emission in this spectral range all but requires observatories in space for its measurement. The all-sky surveys by the cosmological satellites WMAP and COBE provide a unique opportunity to acquire the missing information and complement existing data. In this paper, we have used the COBE and WMAP archive databases to extract maps and globally integrated flux densities for the Clouds. As we will describe below, this resulted, among other things, in the surprising discovery of a significant excess of emission from the Magellanic Clouds at millimeter and sub-millimeter wavelengths.

2. WMAP and COBE maps of the Magellanic Clouds

2.1. WMAP data

The WMAP mission and its data products have been described in detail by Bennett et al (2003a, b, c). For our analysis of the Magellanic Clouds, as in the case of Centaurus A (Israel et al. 2008), we used the reduced and calibrated Stokes I maps of the entire sky from the official WMAP

Table 1. Global Emission from LMC and SMC.

Freq. ν	Wavel. λ	Flux Densities	
		LMC	SMC
WMAP			
(GHz)	(mm)	Jy	
23	13	160±25	17±3
31	9.8	159±25	20±4
41	7.3	165±25	24±5
61	4.9	205±32	40±8
93	3.2	366±65	88±18
COBE-DIRBE			
(THz)	(μm)	Jy	
1.25	240	153000±3000	12350±1440
2.14	140	251100±4500	18900±2005
3.0	100	200200±3000	15750±2125
5.0	60	50500±7500	7010±730
12.0	25	7520±1100	425±70
25.0	12	3450±600	235±35
61.2	4.9	1240±190	150±25
85.7	3.5	2190±300	280±40
136.4	2.2	3765±540	525±65
240.0	1.25	4520±650	670±80

5-year release (Hinshaw et al. 2009). The maps were observed at frequencies $\nu = 22.5, 32.7, 40.6, 60.7,$ and 93.1 GHz with resolutions of 53, 40, 31, 21, and 13 arc-min respectively. The HEALPIX data maps were converted to flat maps in Zenithal Equal Area projection with pixel solid angles of $p(o) = 1.90644 \times 10^{-6}$ sr and intensities in mK. We integrated over the full extent of the LMC and the SMC and determined the flux densities given in Table 1 from the summed values with conversion factors $\text{Jy/mK} = 30.7 \times p(o) \times \nu^2$. In the case of the SMC, we took care to exclude the patch of Milky Way foreground emission at position $-2^\circ, +1.5^\circ$ in Fig. 2. In order to find large-scale regional differences, we also determined flux densities for sub-regions of the Magellanic Clouds, including the 30 Doradus region in the LMC, and the SMC Wing; they are listed in Table 2. The errors quoted are much larger than the formal errors in the integrated flux densities, because we took into account the uncertainty in the required integration area and the uncertainty in the Milky Way foreground contribution. The maps of both Clouds are shown in Figs. 1 and 2 to illustrate noise and confusion levels.

2.2. COBE data

The COBE satellite was launched in 1989 to measure the diffuse infrared and microwave radiation from the early universe (Boggess et al., 1992). It carried three instruments, a Diffuse Infrared Background Experiment (DIRBE), a Differential Microwave Radiometer (DMR), and a Far Infrared Absolute Spectrophotometer (FIRAS).

2.2.1. DIRBE

The DIRBE experiment mapped the sky at wavelengths of 1.25 (*J*), 2.20 (*K*) 3.5 (*L*) 4.9 (*M*), 12, 25, 60, 100, 140, and 240 μm with a 0.7° beam (Silverberg et al. 1993; see also

Wall et al. 1996). We extracted map data in Galactic coordinates for the parts of the sky containing the LMC and the SMC, respectively, and reversed both longitude and latitude directions in order to obtain images corresponding to the sky distribution. On the LMC and the SMC, we extracted cubes of 51×51 and 41×41 pixels in extent, respectively. Each pixel is 0.3 degrees in size. These fields were chosen because they are centred on the lowest believable contour in the $100\mu\text{m}$ maps. In each map, we subtracted both unrelated (stellar) point sources and a smoothed background. Flux densities, determined by integrating over the relevant map areas, are listed in Tables 1 and 3. Fig. 3 shows the distribution of infrared luminosity over the LMC and SMC, as derived from integrating over all DIRBE channels, and also serves a reference for the positions listed in Table 3. Individual channel maps are not shown here¹. The quoted errors are dominated by calibration uncertainties and are significantly larger than the formal random errors.

2.2.2. FIRAS

The FIRAS experiment was designed for precise measurements of the cosmic microwave background spectrum and to observe the dust and line emission from the Galaxy. It covered the wavelength range from 0.1 to 10 mm in two spectral channels and had approximately 5% spectral resolution and a 7° field of view (Wright et al. 1991; Fixsen et al. 1994, 1997). We extracted a continuum spectrum of the LMC, the SMC being too weak. Because the LMC was only marginally resolved by FIRAS, we averaged the spectrum over all pixels within 6 degrees of galactic coordinates (280.47, -32.89). From this, we subtracted an OFF spectrum that was the average of pixels in the annulus from 7 to 12 degrees from the center. We do not list the results for the individual 204 spectral points, but they are shown in Fig. 4.

2.3. Literature data

We have used the IPAC NED as a guide to find LMC and SMC global flux densities over a wide frequency range in the published literature. The NED compilation should be used with care, as it is not complete and also includes values of limited spatial coverage often significantly underestimating total flux densities. Consequently, we also searched the recent literature, and in all cases took care to select only those flux densities that (a) were reliably determined, and (b) correspond to the entire galaxy, not just the bright circumnuclear region.

In addition to the integrated optical flux densities U_T , B_T , and V_T (i.e. not corrected for extinction) from the Third Reference Catalog of Bright Galaxies, (RC 3 – de Vaucouleurs et al. 1991), we have used radio data obtained or collected by Loiseau et al. (1987), Mountfort et al. (1987), Alvarez et al. (1987, 1989), Klein et al (1989), Ye & Turtle (1991), and Haynes et al. (1991). Infrared and sub-millimeter continuum data were taken from Schwering 1988, Rice et al. (1988), Stanimirovic et al. (2000), Aguirre

¹ Foreground-corrected channel images derived from the Zodi-Subtracted Mission Average Maps can be found on Karl Gordon's website <http://dirty.as.arizona.edu/~kgordon/research/mc/mc.html>

Table 2. WMAP peak flux densities in the Magellanic Clouds

Pos ^a Name ^b	LMC								SMC		
	1+2+3 30Dor ^c	4 N206	6 N77-94	7 Bar	8 N11	9 N44	10 N48	12 N57	1 Wing	2 NE	3 SW
ν (GHz)	Flux densities Jy										
23	55 (72)	3.3	6.4	5.2	6.6	4.1	3.2	4.8	2.5	7	7
31	57 (72)	3.6	6.6	5.2	7.5	4.5	2.9	5.1	3	9	8
41	57 (71)	4.2	6.9	5.5	7.9	4.9	2.8	5.3	4	10	10
61	58 (74)	6.7	8.7	6.5	10.5	6.8	2.8	6.7	8	16	16
93	101 (198)	13.1	19.1	10.5	19.3	13.3	4.0	11.5	19	34	35

Notes a. Position numbers correspond to DIRBE position numbers in Table 3, but area covered is not identical. b. Object identifies the most prominent feature within the aperture, usually an HII region complex. c. Numbers in the first column are flux densities with local background level subtracted; numbers in the second column, between parentheses, are flux densities as measured by integrating over the aperture without background subtraction.

Table 3. COBE-DIRBE peak flux densities in the Magellanic Clouds

Pos. ^a Name ^b Pixel	LMC												SMC		
	1 30Dor	2 N159	3 Ridge	4 N206	5 —	6 N77-94	7 Bar	8 N11	9 N44	10 N48	11 N63	12 N57	1 Wing	2 NW	3 SW
λ (μm)	Flux Densities kJy														
1.25	0.174	0.228	0.121	0.113	0.031	0.090	0.315	0.053	0.085	0.047	0.064	0.059	0.102	0.177	0.315
2.2	0.154	0.196	0.098	0.088	0.022	0.076	0.251	0.048	0.066	0.040	0.059	0.046	0.077	0.133	0.238
3.5	0.116	0.126	0.056	0.049	0.013	0.049	0.143	0.032	0.043	0.025	0.035	0.030	0.042	0.071	0.128
4.9	0.084	0.077	0.031	0.028	0.008	0.030	0.081	0.019	0.027	0.015	0.018	0.019	0.023	0.040	0.072
12	0.78	0.41	0.106	0.068	0.026	0.128	0.21	0.095	0.140	0.063	0.040	0.081	0.028	0.060	0.091
25	3.16	1.08	0.114	0.095	0.020	0.25	0.35	0.21	0.29	0.099	0.068	0.186	0.066	0.138	0.180
60	24.9	12.9	1.56	1.74	0.307	3.05	6.04	2.63	4.36	1.43	0.99	2.92	1.21	2.74	3.94
100	35.6	22.1	5.26	4.23	1.24	7.21	11.5	6.39	9.04	3.98	2.69	6.33	3.06	6.06	8.51
140	39.0	26.6	7.92	5.48	2.33	9.03	13.1	7.35	11.1	5.07	3.20	7.17	3.62	6.98	9.47
240	19.2	13.8	5.32	3.19	2.04	6.06	6.79	4.68	6.71	3.36	2.30	4.42	2.68	4.1	5.18
	Luminosity ($10^7 L_{\odot}$)														
1-240	15.6	11.4	3.32	2.74	0.90	3.37	7.29	2.44	4.23	1.77	1.57	2.92	3.21	5.68	8.99
12-240	12.9	8.4	1.79	1.35	0.43	2.14	3.78	1.74	3.07	1.14	0.82	2.05	1.52	2.86	4.07
12-100	9.0	5.3	9.02	0.75	0.18	1.23	2.36	1.02	1.83	0.62	0.46	1.22	8.71	1.69	2.44

Note. a. Position numbers correspond to WMAP position numbers in Table 2, but area covered is not identical. b. The objects refer to the most prominent features included in the aperture. These are the giant HII region complex 30 Doradus (1); the very bright HII region complex N159 south of 30 Dor (2); the prominent ridge of radiating dust and molecular gas south of 30 Dor and N159 (3); the bright but isolated HII region complex N206 south of the LMC Bar (4); a very extended HII region complex, containing N77, N79, N83, N87, N90, N93, N94 at the southwestern corner of the LMC (6); the LMC Bar itself (7); the second brightest HII region complex N11 at the northwestern corner of the LMC (8); the third brightest HII region complex N44 north of the Bar (9); the HII region complexes N48, N63, and N57, delineating Shapley Constellation III (10, 11, 12)

et al. (2003), Wilke et al. (2004), Hughes et al. (2006), Bolatto et al. (2007), and Leroy et al. (2007). The ultraviolet data of the LMC are those of Page and Carruthers (1981). All data used are listed in the on-line appendix.

Comparing the Magellanic Cloud measurements from the WMAP and the DIRBE surveys (Table 1) with published results from other spacecraft (IRAS, ISO, Spitzer) surveys, we note that the infrared peak intensities measured by the COBE-DIRBE experiment for the SMC are very close to these, but somewhat higher for the LMC. As the large extent of the LMC renders its measurement with relatively small beams more sensitive to base-level uncertainties, we prefer the low-resolution DIRBE flux-densities. The

radio continuum spectrum is uncertain below 200 MHz, but well-defined at the higher frequencies. The high-frequency radio continuum measurements agree well with the results from WMAP.

2.4. Comparison galaxies

In the following, we will compare the Magellanic Cloud results to those of other galaxies. However, there are very few galaxies whose emission in the sub-millimeter to centimeter wavelength range has been sampled with a sufficient degree of accuracy and completeness. A more or less exhaustive sample consists of the starburst (SB) disk

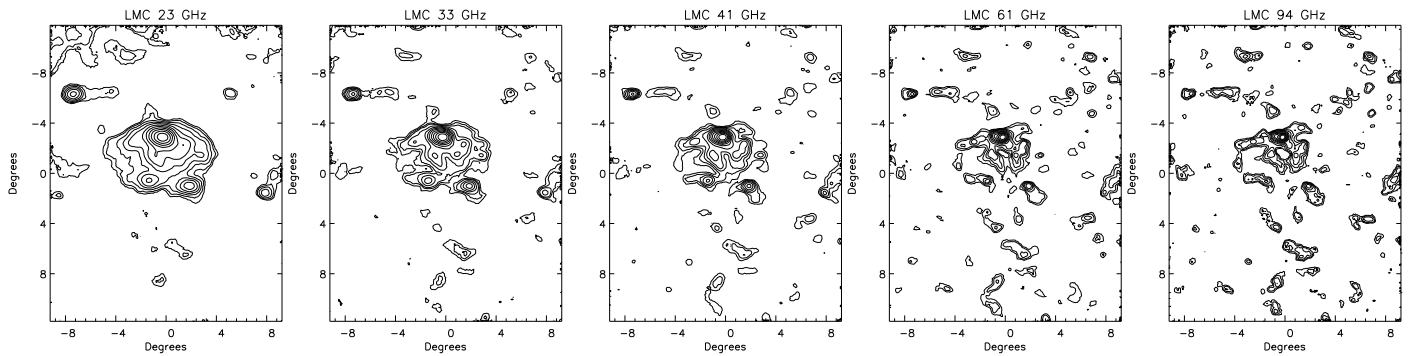


Fig. 1. Maps of the radio continuum emission of the LMC at (left to right) 23, 33, 41 GHz, 61 GHz, and 94 GHz. All images are at the nominal WMAP resolution, and in Galactic coordinates centered on $l = 279.70$, $b = -35.10$. Equatorial North is at right. Contour levels are drawn at (23 GHz) 0.1, 0.19, 0.38, 0.74, 1.4, 2.8, 5.5, 10.7 mK, (33 GHz) 0.1, 0.19, 0.36, 0.68, 1.3, 2.4, 4.6 mK; (41 GHz) 0.1, 0.19, 0.34, 0.64, 1.2, 2.2, 4.1, 7.6 mK; (61 GHz) 0.1, 0.17, 0.31, 0.53, 0.94, 1.6, 2.9, 5.0 mK; (93 GHz) 0.1, 0.16, 0.25, 0.40 0.64 1.0, 1.6, 2.6 mK.

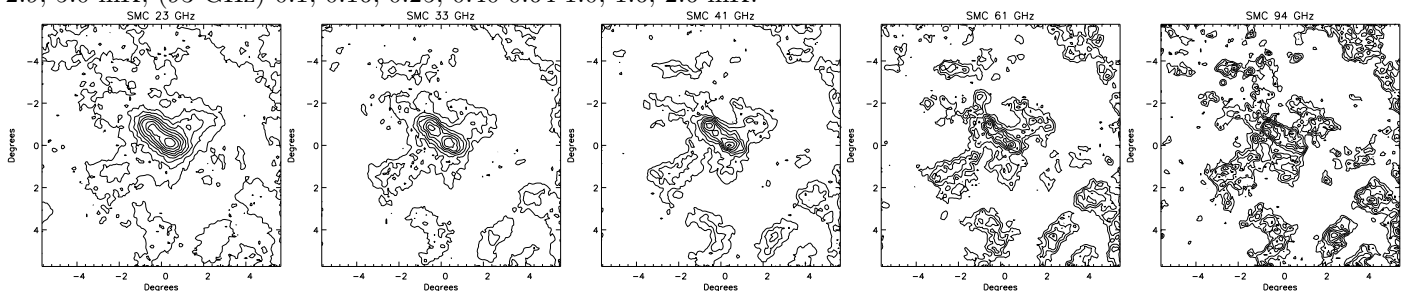


Fig. 2. Maps of the radio continuum emission of the SMC at (left to right) 23, 33, 41 GHz, 61 GHz, and 94 GHz. All images are at the nominal WMAP resolution. Images are in Galactic coordinates, centered on $l = 302.00$, $b = -44.97$, and therefore appear ‘upside-down’; equatorial North is at bottom. Contour levels are drawn at (23 GHz) 0.1, 0.19, 0.38, 0.74, 1.4, 2.8, 5.5, 10.7 mK, (33 GHz) 0.1, 0.19, 0.36, 0.68, 1.3, 2.4, 4.6 mK; (41 GHz) 0.1, 0.19, 0.34, 0.64, 1.2, 2.2, 4.1, 7.6 mK; (61 GHz) 0.1, 0.17, 0.31, 0.53, 0.94, 1.6, 2.9, 5.0 mK; (93 GHz) 0.1, 0.16, 0.25, 0.40 0.64 1.0, 1.6, 2.6 mK.

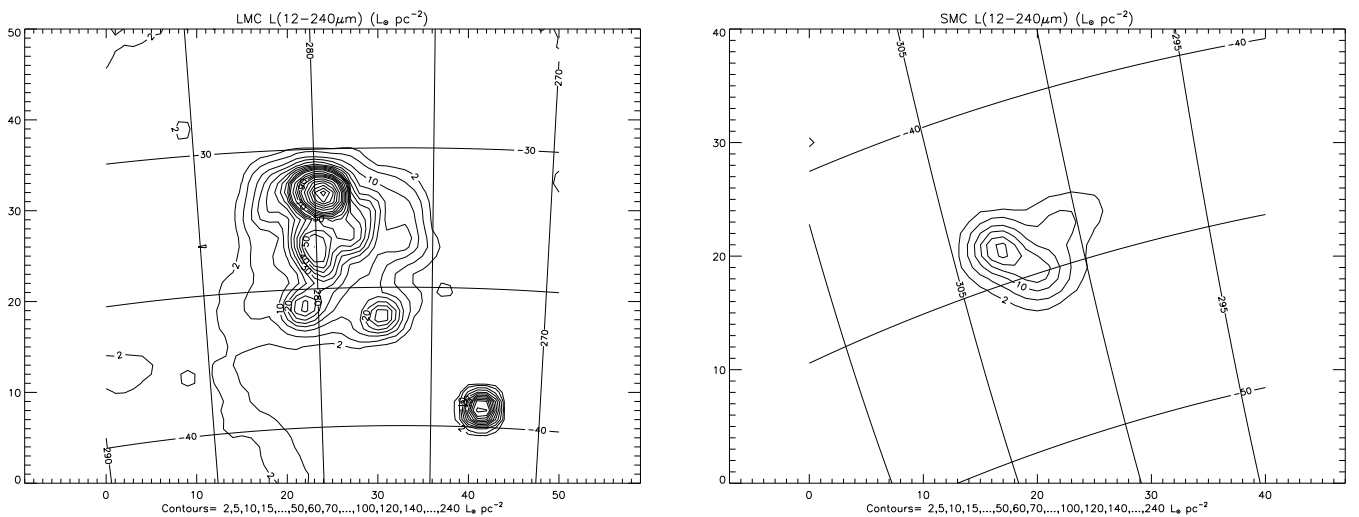


Fig. 3. Total infrared luminosity maps from DIRBE measurements. Contours are marked in units of $L_{\odot} \text{pc}^{-2}$. Galactic coordinates are indicated. Left: LMC. The bright star-forming regions 30 Doradus, N11, and the complex of HII regions N77-N94 are easily identified as is the Bar (cf. Table 3). Bright object at pixel (41,8) is the Galactic foreground star R Dor. Right: SMC. The pixel positions in Table 3 refer to the x and y axis values

galaxies NGC 253, M 82, and NGC 4945 (also measured by WMAP, see Chen & Wright 2009), the (ultra)luminous infrared galaxies (ULIRG) Arp 220, Mk 231, NGC 3690, and NGC 6240, and the star-forming blue compact dwarf (BCDG) galaxies He 2-10, 2Zw40, NGC 4194,

and NGC 5253. The SEDs of these three groups of galaxies will be discussed in more detail in a forthcoming paper.

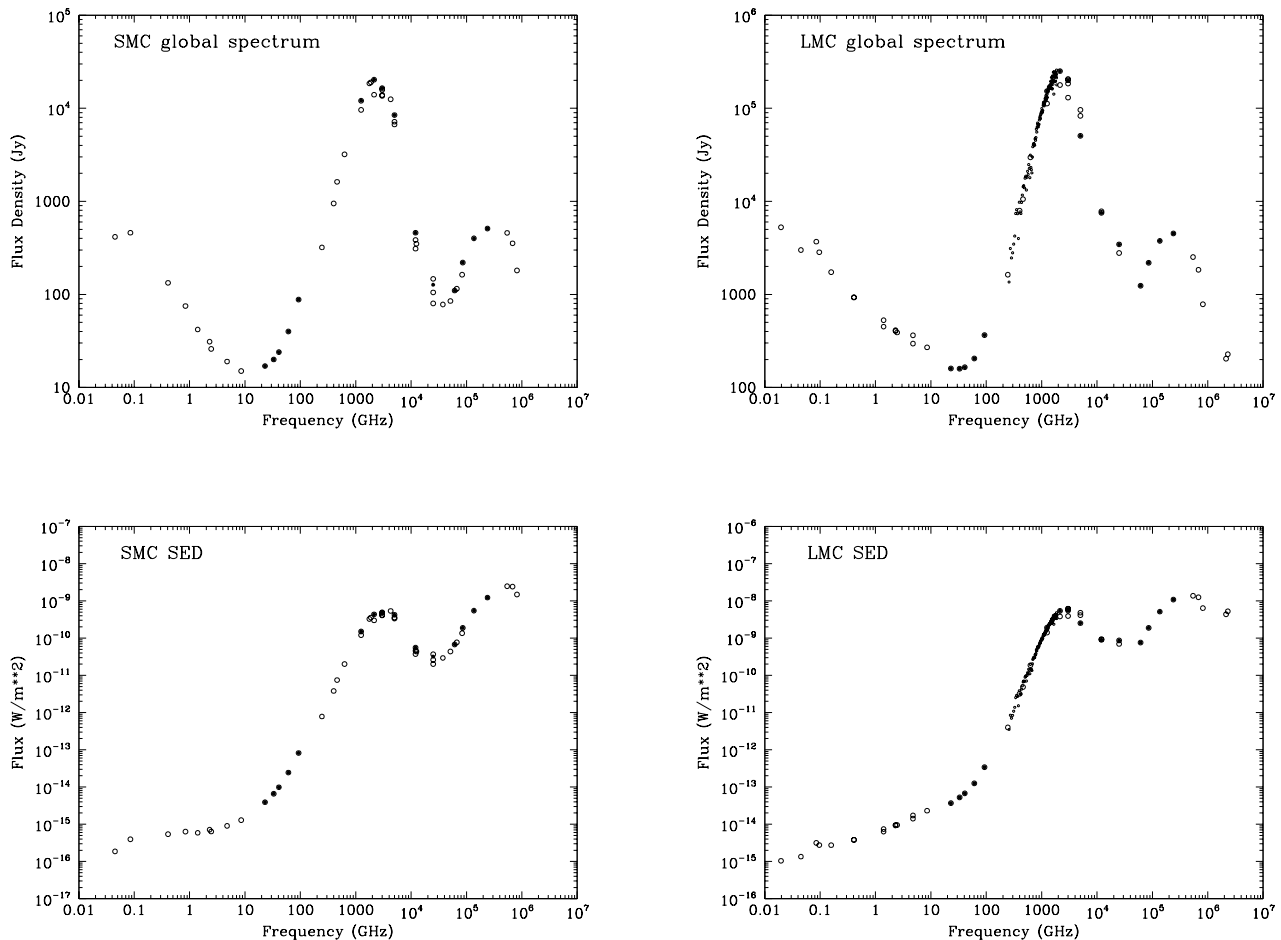


Fig. 4. Top: Global (area-integrated) continuum spectrum from low-frequency radio to the ultraviolet. Filled circles represent integrated flux densities in Jansky from Table 1, open circles were taken from the literature (see text). Bottom: Corresponding global flux (proportional to power) distribution νF_ν in W m^{-2} . Direct starlight is stronger than starlight reemitted by dust, which is the reverse of the usual case in late type galaxies

3. Results and analysis

3.1. Mid-infrared excess emission

From the observed flux density distributions we have determined the mid-infrared excess emission in the $12\mu\text{m}$ broadband by logarithmic interpolation between the observed 4.9μ and 25μ flux densities ($S_{12}/S_{12'}$, with $\log S_{12'} = 0.56 \log S_{25} + 0.44 \log S_5$). Although more precise spectroscopy and photometry has been provided by e.g. the Spitzer Space Observatory (see for instance Draine et al. 2007; Bernard et al. 2008), we include here a brief discussion of the DIRBE data because they allow us to compare the integrated and large scale properties of the Magellanic Clouds to those of other galaxies. Fig. 5 shows that there is no mid-infrared excess in the SMC probably due to decreasing PAH strengths (see e.g. Bolatto et al. 2007). Compared to other galaxies there is only a weak excess in the LMC. The sub-regions of the LMC shown in Fig. 6 reveal the $12\mu\text{m}$ excess to cover a modest but non-negligible range. Low metallicities, hard radiation fields, and strong shocks may destroy the ($8\mu\text{m}$ emitting ionised) PAHs in all but the best-shielded locations (Engelbracht et al. 2005; Micelotta 2009). However,

the $12\mu\text{m}$ excess may also be related to the presence or absence of very small grains – see, for instance, the mid-infrared emission studies of the LMC by Sakon et al. (2006) and by Bernard et al. (2008). Fig. 7 shows that the mid-infrared excess is *anti-correlated* with the energy density of the radiation field as represented by the $100\mu\text{m}/140\mu\text{m}$ flux density ratio (consistent with conclusions by Beirão et al. (2006) from NGC 5253 Spitzer data). The coolest LMC regions in Fig. 7 (numbers 3 and 5 in Table 3) have the highest $12\mu\text{m}$ excess. As the low-metallicity SMC points and the solar-metallicity galaxy points straddle the intermediate metallicity LMC points, it appears that the mid-infrared excess is proportional to metallicity in addition to being inversely proportional to the radiation field.

3.2. Radio spectrum and extinction

3.2.1. Thermal radio contribution

The LMC and SMC spectra in Fig. 4 and Fig. 6 both show a smooth transition from the radio to the infrared with a broad minimum at 20–40 GHz (8–15 mm wavelength) occurring as thermal emission from ionised gas becomes

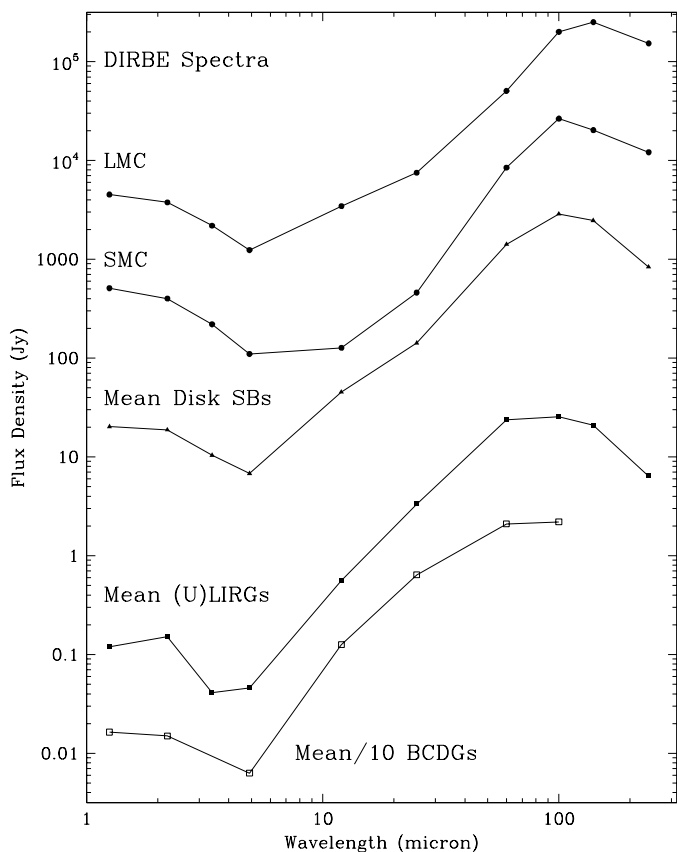


Fig. 5. Near- to far-infrared spectra of the LMC and the SMC, compared to a sample of star-burst galaxies taken from the DIRBE point source catalog by Smith et al. 2004 and data tabulated by Hunt et al. 2005. Most of the galaxies exhibit a clear $12\mu\text{m}$ excess, which is clearly lacking in the SMC and only weakly present in the LMC.

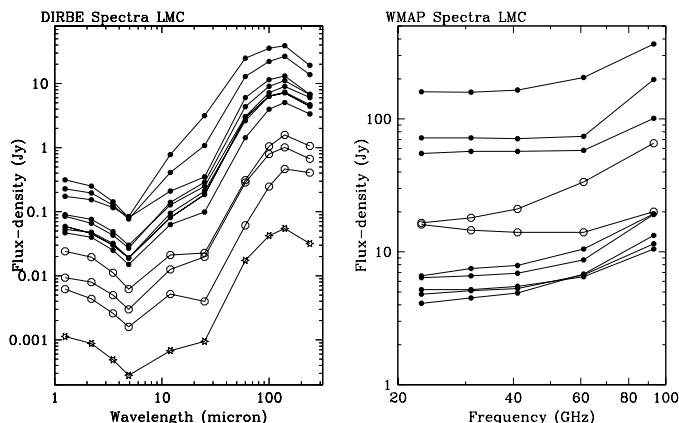


Fig. 6. COBE-DIRBE spectra of the LMC sub-regions from Table 3. For the sake of clarity, we have divided the spectra (open circles) of LMC regions 3 (Dor Ridge), 5, and 10 (N 48) by five, and that of LMC region 4 (N 206; open stars) by a hundred. Right: WMAP spectra of the LMC sub-regions from Table 2). The spectra of the northern source N 48 and the southern object N 206, representing the most extreme cases, have been multiplied by five and are indicated by open circles.

important before the thermal emission from heated dust starts to dominate the energy distribution.

The LMC and SMC radio spectra have spectral indices in the 0.1–5.0 GHz frequency range $\alpha_{LMC} \approx -0.55$ and $\alpha_{SMC} \approx -0.63$ respectively (Alvarez et al. 1987, 1989; Loiseau et al. 1987; Klein et al. 1989; Haynes et al. 1991) with $S_\nu \propto \nu^\alpha$. Such values suggest significant thermal contributions at the highest observed frequencies, but these have been difficult to determine accurately because observations were limited to the spectral range dominated by the non-thermal component. The integrated $H\alpha$ fluxes measured by Kennicutt et al. (1995) together with average foreground extinctions $A_V(LMC) = 0.25$ mag and $A_V(SMC) = 0.12$ mag (Schlegel et al, 1998) place *lower limits* on the thermal contributions of $S_{10GHz}(LMC) \geq 100$ Jy and $S_{10GHz}(SMC) \geq 10$ Jy. The spectra presented in Fig. 4 show that these lower limits are close to the observed total (thermal and non-thermal) flux densities $S_{10GHz}(LMC) \approx 175$ Jy and $S_{10GHz} \approx 14.5$ Jy.

The present data allow us to separate with very high accuracy the thermal and non-thermal contributions by fitting simultaneously the radio spectrum over *both* the range where non-thermal emission dominates *and* the range where thermal emission is dominant. The LMC is best fit by a thermal continuum (spectral index $\alpha = -0.1$) corresponding to $S_{10GHz}(th, LMC) = 145 \pm 15$ Jy. The corresponding 5 GHz thermal fraction is 0.53. For the SMC we find a best fit $S_{10GHz}(th, SMC) = 13.4 \pm 1.0$ Jy, with corresponding 5 GHz thermal fraction of 0.71. Thus, we find in the LMC a substantially lower and in the SMC a substantially higher thermal contribution than estimated by Haynes et al. (1991) from fitting the non-thermally dominated decimeter/centimeter radio data only. Our fits also provide values for the spectral index of the non-thermal emission, $\alpha_{LMC} = -0.70 \pm 0.05$ and $\alpha_{SMC} = -1.09 \pm 0.10$. The Lyman-continuum fluxes $\log N_L = 52.57$ (LMC) and $\log N_L = 51.72$ (SMC) of the ionising star ensembles in the Clouds implied by these thermal flux-densities correspond to the presence of at least 2200 and 300 early O (mean spectral type O6.5, cf. Vacca et al. 1996) in the LMC and the SMC respectively.

3.2.2. Extinction

The free-free radio emission just determined and the integrated $H\alpha$ fluxes ($f_{H\alpha}(LMC) = 9.0 \times 10^{-8}$ erg cm^{-2} s^{-1} and $f_{H\alpha}(SMC) = 1.0 \times 10^{-8}$ erg cm^{-2} s^{-1}) from Kennicutt et al. (1995) accurately define the extinction of the Magellanic Clouds at the wavelength of $H\alpha$ (R -band). Including foreground, we find $A_{H\alpha}(LMC) = 0.65 \pm 0.15$ mag and $A_{H\alpha}(SMC) = 0.45 \pm 0.05$ mag. This is in excellent agreement with the extinction determined for samples of individual HII regions by Bell et al. (2002: mean $A_{H\alpha}(LMC) = 0.62 \pm 0.05$ for 52 objects) and Caplan et al. (1996: mean $A_{H\alpha}(SMC) = 0.50 \pm 0.05$ for 35 HII objects). It follows that the extinction of the diffuse $H\alpha$ emission in both the LMC (35%) and the SMC (41%) (Kennicutt et al. 1995) should also be very similar to the overall extinction. When we correct for the Milky Way foreground, the mean internal R -band extinctions are 0.45 ± 0.15 mag (LMC) and 0.36 ± 0.12 (SMC) mag. The very low mean extinctions of the Clouds are also obvious from the – for late-type galaxies

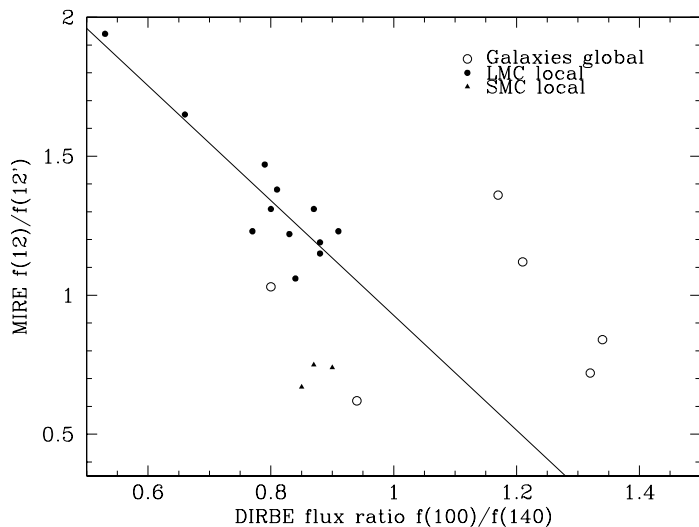


Fig. 7. The mid-infrared excess defined from the COBE-DIRBE measurements (see text) as a function of radiation field energy density. Open symbols represent the global emission from the LMC, the SMC and galaxies taken from the DIRBE point source catalog (Smith et al. 2004). Filled symbols represent sub-regions in the LMC and the SMC, taken from Table 3). The straight line is the linear regression for the LMC sub-regions.

Table 4. Millimeter Excess

Freq. (GHz)	TD	FF	Syn Jy	Excess	Total
LMC: $T_d = 25.0$ K; $\beta = 1.33$					
245	1519	99	12	0	1630
150	328	104	13	55	500
93	64	109	18	175	366
61	17	113	24	51	205
33	2	121	36	0	159
SMC: $T_d = 29.5$ K; $\beta = 0.91$					
245	311	9.0	0.3	0	320
150	81	9.5	0.5	69	160
93	19	10.0	0.9	58	88
61	6.1	10.4	1.4	23	40
33	0.8	11.1	1.7	7	20

Note: TD = Thermal dust emission extrapolated from the spectral fit published by Aguirre et al. (2003); FF = free-free thermal emission; Syn = synchrotron nonthermal emission; Excess = emission in excess over the sum of the preceding contributions, required to make up the observed total emission listed in the last column (the 150 GHz flux being an interpolation). The values for T_d and β were taken from Aguirre et al. (2003).

– unusually low ratios of the far-infrared and optical peaks in their SEDs, $\frac{\nu S_{\nu}^{dust}}{\nu S_{\nu}^{star}} \approx 0.2$ (Fig. 4).

3.3. Millimeter and sub-millimeter excess in the Magellanic Clouds

A major difference between the Magellanic Clouds and the WMAP star-burst galaxies is a significant excess of emission at millimeter and sub-millimeter wavelengths. In the latter, dust emission is the dominant flux contributor only

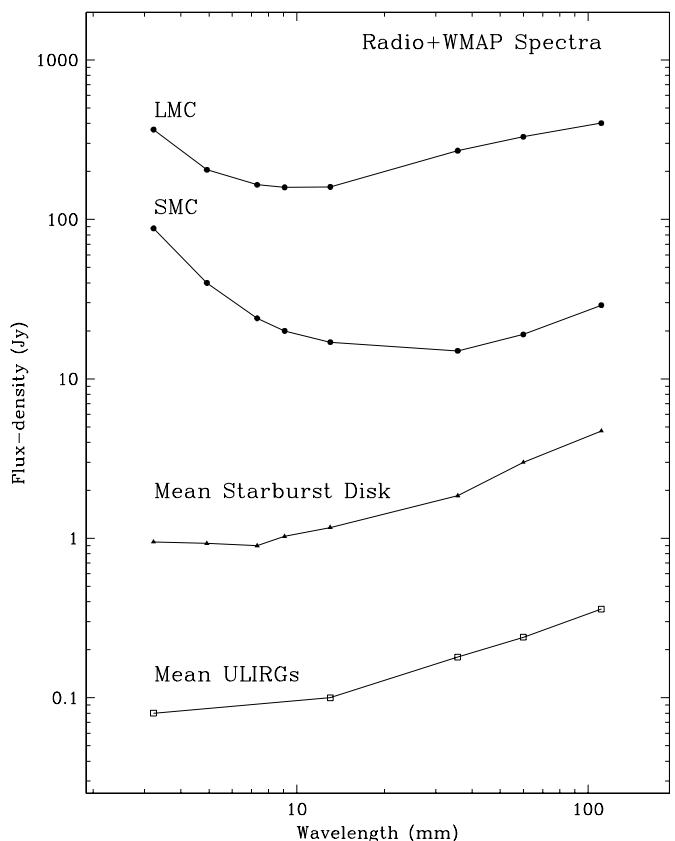


Fig. 8. Millimeter continuum spectra of the Magellanic Clouds compared to the means of other galaxies taken from the WMAP point source catalog (Chen & Wright 2009). WMAP points between 1.3 cm (23 GHz) and 3.2 mm (93 GHz) are supplemented by radio continuum data from 11 cm (2.7 GHz) to 3.6 cm (8.4 GHz) taken from the literature. The spectra of the LMC and the SMC clearly exhibit an upturn extending to relatively long wavelengths (low frequencies) due to the presence of anomalous dust emission. In contrast, the spectra of the star-burst disk galaxies and those of the much more luminous (U)LIRGs show only spectral flattening as free-free emission becomes dominant at short wavelengths.

above 100 GHz (short-wards of 3 mm). In contrast, the spectral upturn associated with dust emission occurs in the LMC and especially the SMC at *much lower* frequencies of 30 GHz (7.5 mm) and 10 GHz (3 cm) respectively (see Fig 8).

3.3.1. LMC and SMC millimeter and sub-millimeter spectra

At sub-millimeter wavelengths, excess emission is known to occur in dwarf galaxies such as NGC 1569 (Lisenfeld et al. 2002; Galliano et al. 2003), II Zw 40, He 2-10, NGC 1140 (Galliano et al. 2005), as well as the star-burst galaxies NGC 3310 (Zhu et al. 2009), and NGC 4631 (Dumke et al. 2004; Bendo et al. 2006). In all these cases, there is a relatively small excess of emission at wavelengths of 0.85 and 1.2 mm over values extrapolated from the far-infrared peak assuming a big grain emissivity $\beta = 2$ (where β is defined by $F_{\nu} \propto B_{\nu}(T_d) \nu^{\beta}$) and related to the Rayleigh-Jeans spectral index by $\beta = \alpha_{FIR} - 2$). The perceived magnitude

of this excess is critically dependent on the quality of the observations and the model extrapolations. The Magellanic Cloud SEDs are much better sampled, and the WMAP observations extend the spectral coverage to millimeter wavelengths, obviating the need for an extrapolation. This leads to a significant improvement in the quality of fits, and thus the determination of excess emission.

The LMC and the SMC exhibit a striking excess at both millimeter and sub-millimeter wavelengths. It is noteworthy that equally well-sampled spectra of the Orion complex in the 1-1000 GHz range (Dicker et al. 2009) show a similar range of turnover frequencies. In the relatively quiet HII region the upturn frequency is at about 100 GHz – as it is in the star-burst galaxies. However, towards the star-forming Orion-KL source, the upturn frequency occurs at 40 GHz, as it does in the LMC. Simultaneously, the dust emissivity changes from $\beta = 2.0$ in the nebula to $\beta = 1.2$ in Orion-KL.

The excess emission manifests itself between 0.3 mm and 10 mm (30 GHz and 1000 GHz) as a combination of a relatively low upturn frequency (defined as the frequency of minimum emission in the millimeter spectral range, ν_{mm}^{min}) and a relatively low sub-millimeter spectral index α_{FIR} , i.e. a relatively low emissivity β around unity. There are two obvious ways in which the dust emission upturn will shift to lower frequencies (longer wavelengths) in any spectrum without the need to invoke special properties of the radiating dust. First, if the radio continuum is unusually *weak* with respect to the far-infrared emission from dust, the downshift of the radio part will quite naturally cause the point where dust becomes dominant (the upturn) to shift to lower frequencies. This is not the case as the Magellanic Clouds have, in fact, a relatively strong radio continuum. The comparison galaxies from Sect. 2.4 (included in Fig. 8 have (much) larger $\frac{S_{dust}^{max}}{S_{min}^{min}}$ ratios (2000-3000) than the Magellanic Clouds (1650 and 1200) but do not exhibit a lower upturn frequency. Second, if the same far-infrared emission peak occurs at a lower frequency, the Rayleigh-Jeans tail is displaced to lower frequencies by the same amount, also causing the upturn to occur earlier. In the Magellanic Cloud, the far-infrared peak indeed occurs at somewhat longer wavelengths λ_{dust}^{max} (lower frequencies) than in most other galaxies but not by the amount needed to explain the observed low upturn frequencies ν_{mm}^{min} .

We refer to Fig. 6 of Leroy et al. (2007) to illustrate that the SMC spectrum is much flatter than the canonical $\beta = 2$ spectrum. It is even in excess of the $\beta = 1.5$ model spectrum, and the longest-wavelength data point at 1200 μm suggests further flattening. The same situation applies to the LMC spectrum. In addition to the unmistakable sub-millimeter excess of the LMC and the SMC, the data presented in this paper show *a further millimeter excess*.

We have quantified this additional millimeter excess by calculating at four frequencies the combined emission of the non-thermal radio, thermal radio, and thermal dust components. For the former, we extrapolated the results from the preceding discussion; for the latter we extrapolated the spectral fits to the DIRBE and TopHat data published by Aguirre et al. (2003) in their Fig. 4 and Table 9, assuming no additional excess to be present at their lowest frequency of 245 GHz (longest wavelength of 1200 μm). Our results are given in Table 4, which shows a significant excess (about

50% of the total emission at 93 GHz) in the LMC, and an even stronger excess in the SMC at all mm wavelengths.

3.3.2. Possible explanations for a (sub)millimeter excess

Various dust emission mechanisms have been suggested in order to explain excess emission at millimeter and shorter wavelengths.

(i) *Very cold big dust grains.* Any far-infrared/sub-millimeter dust emission spectrum can be modelled by a sufficient number of modified black-body curves each representing a population of big grain dust particles in thermal equilibrium at a particular dust temperature. An emissivity $\beta = 2$ is commonly assumed, although an inverse temperature dependence $\beta = (0.40 + 0.008 T_d)^{-1}$ has been proposed by Dupac et al. (2003). The values $\beta \approx 1.7$ characterising the star-burst disk galaxies correspond to mean dust temperatures $T_d \approx 25$ K. However, any such fit of the FIR/sub-mm spectra of the Magellanic Clouds requires the additional presence of a significant component of very cold dust ($T_d \ll 10\text{K}$, approaching 3 K). At such low temperatures, very large amounts of cold dust are required to produce even a modest amount of excess emission. Regarding other galaxies for which a sub-millimeter excess was surmised, virtually all (Lisenfeld et al. 2002; Dumke et al. 2004; Bendo et al. 2006; Zhu et al. 2009) authors have rejected this solution as they consider the implied great masses of cold dust and the resulting low gas-to-dust ratios to be implausible, in addition to the difficulty of finding large amounts of very cold dust precisely in those environments where low metallicities provide the least shielding against strong ambient radiation fields. These arguments apply here as well. The SMC has a lower metallicity than the LMC, yet it shows a higher excess. It is hard to imagine how it could be richer in cold dust.

A more detailed look at the distribution of WMAP emission over the Clouds (Fig. 6) suggests the same conclusion. There is more excess emission from the bright star-forming regions 30 Doradus, N 11, N 44 than from the LMC Bar and the quiescent northern edge near N 48, although the field centered on the moderately bright southern region N 206 exhibits the highest excess. In the SMC, the NE and SW Bar regions are of very different appearance but show practically identical spectra; the SMC Wing has the steepest spectrum. It is hard to see how these patterns could correspond to the distribution of very cold dust in either galaxy.

(ii) *Different dust grain composition or structure.* The Magellanic Clouds may host a population of dust grains with optical properties very different from those of the dust grains in more metal-rich galaxies. Structurally different dust grains, such as fluffy or fractal particles (Ossenkopf & Henning 1994; Paradis et al. 2009) could produce the sub-millimeter excess. In fact, Reach et al. (1995) propose this to be the explanation for the widespread cold dust component they found in the Milky Way from COBE/FIRAS measurements, after rejecting either very cold big dust grains or very small grains as a possibility.

The dust grain emissivity β is not only a function of dust temperature, but it also depends on the grain composition. For instance, amorphous graphite has $\beta = 1$ whereas crystalline dust has $\beta = 2$ (Mennella et al. 1998; Agladze et al. 2005). Thus, we cannot exclude in low-metallicity star-forming galaxies such as the LMC and the SMC the predominance of a dust grain population with different op-

tical properties causing β to be around unity, or even the inconspicuous presence of such dust in more massive metal-rich spiral galaxies (such as the Milky Way, cf. Reach et al. 1995). However, it is not clear what this population is (but see Mény et al. 2007), or what processes would lie at the root of its dominance in both star-forming dwarf galaxies and more extreme (ultra)luminous infrared galaxies, nor is it obvious that β could be as low as zero, as appears to be the case in the SMC.

(iii) *Very small spinning dust grains*, first modelled by Draine & Lazarian (1998), have been invoked to explain anomalously high and apparently dust-correlated microwave emission in the WMAP Milky Way foreground, and Murphy et al. (2009) have suggested that such grains are also present in the nearby spiral galaxy NGC 6946. Recently, Ali-Haïmoud et al. (2009) and Dobler et al. (2009) have suggested that this peak frequency may occur anywhere between 30 GHz and 50 GHz, but the spectra in Fig. 4 lack a maximum around these frequencies. However, the WIM presented by these authors may not be representative of what is expected in the Magellanic Clouds, as they calculated spinning dust emissivities for grains illuminated by an ISRF with intensity $U = 1$ (Mathis et al. 1983). In actual fact, the IR modelling of the SMC and LMC SEDs requires a distribution of radiation field intensities from $U = 0.1$ -0.8 to 1000. This may shift the peak to much higher frequencies up to 100 GHz (Ysard & Verstraete 2009, and Ysard et al. 2009). The possibility that the LMC and SMC excess involves spinning dust cannot be excluded, and is explored in more detail in a companion paper (Bot et al. 2010)

The presence of the excess emission in the Magellanic Cloud sub-millimeter spectrum has an important consequence. As long as its nature is unidentified, it is impossible to ascertain the degree to which it ‘contaminates’ the Rayleigh Jeans tail of the far-infrared dust emission. *It follows that fitting existing dust emission models to this tail will not provide information on the amount of dust much cooler than that responsible for the far-infrared emission peak, i.e. on dust radiating at temperatures below $\approx 15 - 20$ K. As even large amounts of cold dust contribute only modest amounts of emission, the apparently indeterminate nature of the Rayleigh-Jeans tail renders reliable determination of total dust mass and gas-to-dust ratio impossible.*

The Magellanic Clouds (and other star-forming dwarf irregular galaxies) differ in a number of ways from more massive galaxies, such as the Milky Way, M 82, NGC 253, in their dust-related properties. In addition to the pronounced millimeter and sub-millimeter excess emission and the weaker $12\mu\text{m}$ emission, they have (a) lower metallicities, (b) fewer PAHs, (c) much lower total extinction, (d) much weaker $\lambda 2175\text{\AA}$ extinction features, and (e) more steeply rising UV extinction curves. In *all* these respects, the SMC is more extreme than the LMC, and they appear to be related in some way. A common denominator may be metallicity-related modifications of individual dust grains or the global dust population, or both.

4. Summary and conclusions

1. We have extracted from the COBE-DIRBE and WMAP databases maps of the Large and the Small Magellanic Cloud in the $1.25\ \mu\text{m} - 240\ \mu\text{m}$ and $23\ \text{GHz} - 93\ \text{GHz}$ spectral ranges respectively. We have used the maps to determine globally integrated flux densities.
2. We complemented the COBE-DIRBE and WMAP flux densities by those literature flux densities that reliably represent the global emission from the Clouds. We used the resulting data sets to construct the flux density and energy distributions over the full spectral range from low-frequency radio to ultraviolet, for the first time covering the critical three spectral decades in the sub-millimeter-to-centimeter window ($10\ \text{GHz} - 1\ \text{THz}$).
3. We have established that the SMC and the LMC have significant emission above the expected free-free radio continuum starting at frequencies of $10\ \text{GHz} - 30\ \text{GHz}$ and extending over millimeter and sub-millimeter wavelengths into the far-infrared.
4. The excess is not caused by cold, big dust grains. The existence of the excess emission will provide new insight in the nature of interstellar dust, but in the meantime renders impossible reliable determination of total dust mass as well as gas-to-dust ratio.
5. The free-free thermal radio continuum is $13.4(\nu/10\text{GHz})^{-0.1}$ Jy for the SMC, and $146(\nu/10\text{GHz})^{-0.1}$ Jy for the LMC, implying Lyman continuum fluxes $\log N_L = 51.72$ and $\log N_L = 52.57$, respectively.
6. The mean visual extinctions internal to the SMC and the LMC are $A_V^{int} = 0.45$ mag and $A_V^{int} = 0.56$ mag respectively, in addition to Milky Way foreground extinctions of 0.12 mag and 0.25 mag.

References

- Agladze N.I., Sievers A.J., Jones S.A., Burlitch J. M., & Beckwith S.V.W., 1996, ApJ 462, 1026
- Aguirre J.E., Bezaire J.J., Cheng E.S., Cottingham D.A., Cordone S.S., and 8 coauthors, 2003, ApJ 596, 273
- Ali-Haïmoud Y., Hirata C.M., & Dickinson C., 2009, MNRAS 395, 1055
- Alvarez H., Aparici J., & May J., 1987 A&A 176, 25
- Alvarez H., Aparici J., & May J., 1989 A&A 213, 13
- Alvarez H., Aparici J., May J., & Reich P., 2000 A&A 355, 863
- Beirão P., Brandl B.R., Devost D., Smith J.D., Hao L., & Houck J.R., 2006, ApJL 643, L1
- Bell E.F., Gordon K.D., Kennicutt R.C., & Zaritsky D., 2002, ApJ 565, 994
- Bendo G.J., Dale D.A., Draine B.T., et al. 2006, ApJ 652, 283
- Bennett C. L., Bay M., Halpern M., and 12 coauthors, 2003a, ApJ 583, 1
- Bennett C. L., Halpern M., Hinshaw G., and 18 coauthors, 2003b, ApJS 148, 1
- Bennett C. L., Hill R. S., Hinshaw G., and 13 coauthors, 2003c ApJS 148, 97
- Bernard J.-P., Reach W.T., Paradis D., and 46 coauthors, 2008, AJ 136, 919
- Boggess N. W., Mather J. C., Weiss R., Bennett C. L., Cheng E. S., Dwek, E., and 12 coauthors, 1992, ApJ 397, 420
- Bolatto A.D., Simon J.D., Stanimirovic S., Van Loon, J.T., Shah, R.Y., and 10 coauthors, 2007 ApJ 655, 212
- Bot C., Ysard N., Paradis D., Bernard J.-P., Lagache G., Israel F.P., & Wall W.F., 2010, A&A , submitted
- Caplan J., Ye T., Deharveng L., Turtle A.J., & Kennicutt R.C., 1996, A&A 307, 403
- Chen X., & Wright E.L., 2009, ApJ 694, 222
- De Vaucouleurs G., De Vaucouleurs A., Corwin H.G., Buta, R. J., Paturel, G., & Fouque, P., 1991, Third Reference Catalogue of Bright Galaxies, version 3.9
- Dicker S.R., Mason B.S., Korngut P.M., & 13 other authors, 2009, arXiv:0907.1300
- Dobler G., Draine B., & Finkbeiner D.P., 2009, ApJ 699, 1374
- Draine B.T., & Lazarian A., 1998, ApJ , 508, 157

- Draine B. T., Dale D. A., Bendo G., and 17 coauthors, 2007, *ApJ* 663,866
- Dumke M., Krause M., & Wielebinski R., 2004, *A&A* 414, 475
- Dupac X., Bernard J.-P., Boudet N., Giard M., Lamarre J.-M., Mény C., Pajot F., Ristorcelli I., Serra G., Stepnik B., & Torre J.-P., 2003, *A&A* 404, L11
- Engelbracht C.W., Gordon K., Rieke G.H., Werner M.W., Dale D.A., & Latter W.B., 2005, *ApJL* 628, L29
- Fixsen D. J., Cheng E. S., Cottingham D. A., Eplee R. E., Hewagama T., and 15 coauthors, 1994, *ApJ* 420, 457
- Fixsen D. J., Weiland J. L., Brodd S., Hauser M. G., Kelsall T., and 5 coauthors, 1997, *ApJ* 490, 482
- Galliano F., Madden S.C., Jones A.P., et al., 2003, *A&A* 407, 159
- Galliano F., Madden S.C., Jones A.P., Wilson C.D., & Bernard J.-P., 2005, *A&A* 434, 867
- Haynes R.F., Klein U., Wayte S.R., Wielebinski R., Murray J.D., and 7 coauthors, 1991, *A&A* 252, 475
- Hinshaw G., Weiland J. L., Hill R. S., Odegard N., Larson D., and 16 coauthors, 2009, *ApJS* 180, 225
- Hughes A., Wong T., Ekers R., Staveley-Smith L., Filipovic M., and 3 coauthors, 2006 *MNRAS* 370, 363
- Hunt L., Bianchi S., & Maiolino R., 2005, *A&A* 434, 849
- Israel F.P., Raban D., Booth R.S., & Rantakyrö F.T., 2008, *A&A* 483, 741
- Kennicutt R.C., Bresolin F., Bomans D.J., Bothun G.D., Thompson I.B., 1995, *AJ* 109, 594
- Klein U., Wielebinski R., Haynes R.F., & Mail D.F., 1989, *A&A* 211, 280
- Leroy A., Bolatto A., Stanimirovic S., Mizuno N., Israel F.P., & Bot C., 2007 *ApJ* 658, 1027
- Lisenfeld U., Israel F.P., Stil J.M., & Sievers A., 2002, *A&A* 382, 860
- Loiseau N., Klein U., Greybe A., Wielebinski R., & Haynes R.F., 1987, *A&A* , 178, 62
- Mathis J.S., Mezger P.G., & Panagia N., 1983, *A&A* 128, 212
- Mennella V., Brucato J.R., Colangeli L., Palumbo P., Rotundi A., & Bussolletti E., 1998, *ApJ* 496, 1058
- Mény C., Gromov V., Boudet N., Bernard J.-Ph., Paradis D., & Nayral C., 2007, *A&A* 468, 171
- Mountfort P.I., Jonas J.L., de Jager G., & Baart E.E., 1987, *MNRAS* 226, 917
- Micelotta E.R., 2009, Ph.D. Thesis, Leiden University
- Murphy E. J., Helou G., Condon J. J., Schinnerer E., Turner J. L., Beck R., Mason B. S., Chary R.-R., & Armus L., 2010, *ApJ* 709 108
- Ossenkopf V., & Henning Th., 1994, *A&A* 291, 943
- Page T., & Carruthers G.R., 1981, *ApJ* 248, 906
- Paradis D., Bernard J.-Ph., & C. Mény, 2009, *A&A* , preprint, <http://dx.doi.org/10.1051/0004-6361/20081246>
- Reach W.T., Dwek E., Fixsen D.J., et al. 1995, *ApJ* 451, 188
- Rice W., Lonsdale C.J., Soifer B.T., and 5 coauthors, 1988, *ApJS* 68, 91
- Sakon I., Onaka T., Kaneda H., and 8 coauthors, 2006, *ApJ* 651, 174
- Schlegel D.J., Finkbeiner D.P., & Davis, M., 1998 *ApJ* 500, 525
- Schwering P.B.W., 1988 Ph.D. thesis Sterrewacht Leiden, Leiden University (NL)
- Shain C. A., 1959 in: *IAU Symp. no. 9*, Ed. R.N. Bracewell, Stanford Univ. Press (Stanford, CA), p. 328
- Silverberg R.F., Hauser M.G., Boggess N.W., Kelsall T.J., Moseley S.H., & Murdock T.L., 1993 *SPIE* 2019, 180
- Smith B.J., Price S.D., & Baker R.I., 2004. *ApJS* 154, 673
- Stanimirovic S., Staveley-Smith L., Van der Hulst J.M., Bontekoe T.R., Kester D.J.M., & Jones P.A., 2000 *MNRAS* 315, 791
- Vacca W.D., Garmany C.D., & Shull J.M., 1996, *ApJ* 460, 914
- Wall W. F., Reach W. T., Hauser M. G., Arendt R. G., Weiland J. L., and 8 coauthors, 1996, *ApJ* 456, 566
- Wilke K., Klaas U, Lemke D., Mattila K., Stickel M., & Haas M., 2004, *A&A* 414, 69
- Wright E. L., Mather J. C., Bennett C. L., Cheng E. S., Shafer R. A., and 17 coauthors, 1991, *ApJ* 381, 200
- Ye T., & Turtle A.J., 1991 *MNRAS* 249, 693
- Ysard N., & Verstraete L., 2009, arXiv0906.3102
- Ysard N., Miville-Deschenes M.-A., & Verstraete L., 2009 arXiv0906.3360
- Zhu M., Papadopoulos P.P., Xilouris E.M., Kuno N., & Lisenfeld U., 2009, arXiv:0908.1600

Appendix A: Spectral data used

Table A.1. Large Magellanic Cloud

Freq. ν (GHz)	Wavel. λ (mm)	Flux Densities		Reference
		Jy	Δ Jy	
0.0197	15230	5270	1054	Shain ^a 1959
0.045	6670	2997	450	Alvarez et al. 1987
0.0855	3510	3689	400	Mills 1959 ^a
0.0968	3100	2839	600	Mills 1959 ^a
0.158	1900	1736	490	Mills 1959 ^a
0.408	735	925	30	Klein et al. 1989
0.408	735	934	173	Haslam et al. 1981 ^a
1.4	214	529	30	Klein et al. 1989
1.4	214	450	30	Hughes et al. 2006
2.3	130	404	30	Klein et al. 1989
2.3	130	412	50	Mountfort et al. 1987
2.45	122	390	20	Haynes et al. 1991
4.75	63	363	30	Haynes et al. 1991
4.75	63	296	25	Hughes et al. 2006
8.55	35	270	35	Haynes et al. 1991
23	13	160	25	This Paper 2010
33	9.1	159	25	This Paper 2010
41	7.3	165	25	This Paper 2010
61	4.9	205	32	This Paper 2010
93	3.2	366	65	This Paper 2010
245	1.2	1630	170	Aguirre et al. 2003
400	0.75	7930	590	Aguirre et al. 2003
460	0.65	10570	890	Aguirre et al. 2003
630	0.48	29660	2980	Aguirre et al. 2003
1250	0.24	112300	2400	Aguirre et al. 2003
1250	0.24	153000	3000	This Paper 2010
2140	0.14	177700	3800	Aguirre et al. 2003
2140	0.14	251100	4500	This Paper 2010
3000	0.10	130100	17600	Aguirre et al. 2003
3000	0.10	200200	3000	This Paper 2010
3000	0.10	206250	30000	Hughes et al. 2006
3000	0.10	184687	28000	Rice et al. 1988
5000	0.06	82917	12000	Rice et al. 1988
5000	0.06	50500	7500	This Paper 2010
5000	0.06	96250	14000	Hughes et al. 2006
12000	0.025	7824	1200	Rice et al 1988
12000	0.025	7520	1100	This Paper 2010
25000	0.012	2782	400	Rice 1988
25000	0.012	3450	600	This Paper 2010
61220	0.0049	1240	190	This Paper 2010
85710	0.0035	2190	300	This Paper 2010
136365	0.0022	3765	400	This Paper 2010
240000	0.00125	4520	650	This Paper 2010
542000	0.00055	2520	139	de Vaucouleurs et al. 1991
681000	0.00044	1840	87	de Vaucouleurs et al. 1991
819000	0.000365	783	53	de Vaucouleurs et al. 1991
2142850	0.00014	204	40	Page & Carruthers 1981
2307700	0.00013	228	45	Page & Carruthers 1981

Note: ^a As revised and listed by Klein et al. 1989

Table A.2. Small Magellanic Cloud

Freq. ν (GHz)	Wavel. λ (mm)	Flux Densities		Reference
		Jy	Δ Jy	
0.0197	15230	5270	1054	Shain 1959; cf Alvarez et al. 1989
0.045	6670	415	80	Alvarez et al 1989
0.0855	3510	460	200	Mills 1959 ^a
0.408	735	133	10	Haslam 1982 ^a
0.843	356	75	8	Ye and Turtle 1991
1.4	214	42	6	Loiseau et al. 1987 ^b
2.3	130	31	6	Mountfort et al. 1987
2.45	122	26	3	Haynes et al 1991
4.75	63	19	4	Haynes et al 1991
8.55	35	15	4	Haynes et al 1991
23	13	17	3	This Paper 2010
33	9.1	20	4	This Paper 2010
41	7.3	24	5	This Paper 2010
61	4.9	40	8	This Paper 2010
93	3.2	88	18	This Paper 2010
245	1.2	320	80	Aguirre et al. 2003
400	0.75	950	190	Aguirre et al. 2003
460	0.65	1620	290	Aguirre et al. 2003
630	0.48	3200	810	Aguirre et al. 2003
1250	0.24	12070	540	Aguirre et al. 2003
1250	0.24	12350	1440	This Paper 2010
1250	0.24	9600	4400	Stanimirovic et al. 2000
1765	0.17 1	18500	4000	Wilke et al 2004 ^c
1875	0.16	19000	4300	Leroy et al.2007
2140	0.14	20300	920	Aguirre et al. 2003
2140	0.14	18900	2005	This Paper 2010
2140	0.14	14000	5600	Stanimirovic et al. 2000
3000	0.10	16480	2220	Aguirre et al. 2003
3000	0.10	15750	2125	This Paper 2010
3000	0.10	13600	930	Stanimirovic et al. 2000
3000	0.10	13900	1810	Schwering 1988
4285	0.07	12500	2400	Leroy et al.2007
5000	0.06	8450	730	This Paper
5000	0.06	6700	1060	Stanimirovic et al. 2000
5000	0.06	7170	957	Schwering 1988
12500	0.024	350	50	Leroy et al. 2007
12000	0.025	460	180	Stanimirovic et al. 2000
12000	0.025	425	70	This Paper
12000	0.025	310	170	Stanimirovic et al. 2000
12000	0.025	385	56	Schwering 1988
25000	0.012	80	30	Stanimirovic et al. 2000
25000	0.012	105	30	Stanimirovic et al. 2000
25000	0.012	147	26	Stanimirovic et al. 2000
25000	0.012	235	25	This Paper 2010
37500	0.008	78	8	Bolato et al. 2007
51274	0.0058	85	9	Bolato et al. 2007
61220	0.0049	110	43	Stanimirovic et al. 2000
61220	0.0049	150	25	This Paper 2010
66667	0.0045	115	12	Bolato et al. 2007
83333	0.0036	163	16	Bolato et al. 2007
85710	0.0035	220	31	Stanimirovic et al. 2000
85710	0.0035	280	40	This Paper 2010
136365	0.0022	400	37	Stanimirovic et al. 2000
136365	0.0022	525	65	This Paper 2010
240000	0.00125	510	25	Stanimirovic et al. 2000
240000	0.00125	670	80	This Paper 2010
542000	0.00055	458	46	de Vaucouleurs et al. 1991
681000	0.00044	354	34	de Vaucouleurs et al. 1991
819000	0.000365	181	22	de Vaucouleurs et al. 1991

Notes: ^a As revised and listed by Loiseau et al. (1987); ^b As revised and listed by Haynes et al. (1991); ^c As revised by Leroy et al. (2007)